JOURNAL OF GEOPHYSICAL RESEARCH, VOL. 99, NO. A11, PAGES 21,291–21,301, NOVEMBER 1, 1994

Nonlinear standing shear Alfvén waves in the Earth's magnetosphere

R. Rankin, P. Frycz, V. T. Tikhonchuk,[1] and J. C. Samson

Department of Physics, Canadian Network for Space Research, University of Alberta, Edmonton Alberta, Canada

Abstract. We present theory and numerical simulations of strong nonlinear effects in standing shear Alfvén waves (SAWs) in the Earth's magnetosphere, which is modeled as a finite size box with straight magnetic lines and (partially) reflecting boundaries. In a low β plasma it is shown that the ponderomotive force can lead to large-amplitude SAW spatial harmonic generation due to nonlinear coupling between the SAW and a slow magnetosonic wave. The nonlinear coupling leads to secularly growing frequency shifts, and in the case of driven systems, nonlinear dephasing can lead to saturation of the driven wave fields. The results are discussed in the context of their possible relevance to the theory of standing ionospheric cavity wave modes and field line resonances in the high-latitude magnetosphere.

1. Introduction

Shear Alfvén waves (SAW) form an important part of the dynamics of the Earth's magnetosphere where they provide an energy transfer process for damping of large scale solar wind perturbations and magnetopause generated compressional waves. The decay processes for these waves can produce small scale magnetic field disturbances in the polar magnetosphere which energize particles and lead to a variety of auroral phenomena. In space physics the study of the effects produced by Alfvén waves has a long history, largely due to the fact that there have been a great many observations of these waves in the solar wind, and in the Earth's magnetosphere and ionosphere. Observations of large-amplitude waves in the solar wind [*Belcher and Davis*, 1971] have stimulated a number of theoretical studies of the nonlinear evolution of Alfvén waves [*Barnes and Hollweg*, 1974; *Cohen and Kulsrud*, 1974; *Granik* 1981], and have resulted in the study of related effects such as parametric instabilities, including the modulation and decay instabilities [*Lashmore-Davies*, 1976; *Sakai and Sonnerup*, 1983; *Wong and Goldstein*, 1986].

Boehm et al. [1990] have observed very large amplitude Alfvén waves at altitudes of 1000 km or so in the auroral ionosphere. The observed frequencies of the waves are typically greater than 1 Hz, and their electric fields correspond to roughly 200 mV/m. These Alfvén waves may be a manifestation of the standing ionospheric cavity wave modes proposed by *Trakhtengertz and Feldstein* [1984] and *Lysak* [1991], who suggested that the wave modes might reach large enough amplitudes for nonlinear effects to become important. *Li and Temerin* [1993] and *Boehm et al.* [1990] have suggested that spatial gradients in the envelopes of the wave fields can lead to ponderomotive forces that produce density enhancements and depletions that are large enough to account for those seen in the magnetosphere.

ULF (1-5 mHz) shear Alfvén field line resonances (FLRs) are also commonly observed in the Earth's magnetosphere and in the auroral ionosphere [*Ruohoniemi et al.*, 1991; *Samson et al.*, 1992]. The equatorial velocity fields of these FLRs can be as large as 200 km/s [*Mitchell et al.*, 1990]. *Samson et al.* [1992] and *Rankin et al.* [1993a] have shown that these large amplitude FLRs should be nonlinearly unstable to the Kelvin-Helmholtz instability in the equatorial plane. The importance of ponderomotive forces in standing Alfvén waves has recently been recognized by *Allan* [1993] and *Li and Temerin* [1993], who attributed them to a mechanism for the differential acceleration of auroral particles and species redistribution.

Alfvén waves can show manifestations of two distinct nonlinear phenomena, harmonic generation and instabilities, which may distort the wave fields and lead to saturation of the amplitudes of the waves. The first of these effects is generally much stronger in standing Alfvén waves than in propagating waves because of larger spatial gradients in the direction of the ambient magnetic field. The second class of nonlinearity includes instabilities such as the Kelvin-Helmholtz instability [*Samson et al.*, 1992, *Rankin et al.*, 1993a] and the nonlinear tearing instability [*Samson et al.*, 1992; *Seyler*, 1990], which might also play a major role in the nonlinear evolution of standing shear Alfvén wave resonances in the Earth's magnetosphere. Instabilities generally require very large amplitude wave fields and

[1] On leave from P. N. Lebedev Physics Institute, Russian Academy of Sciences, Moscow.

Paper number 94JA01629.
0148-0227/94/94JA-01629$05.00

must evolve from initially small amplitude disturbances. However, harmonic generation may evolve faster initially, and the question to be addressed is whether nonlinear harmonic generation can prevent the wave fields from reaching amplitudes that are large enough to exceed instabilty criteria.

In this paper we would like to address the effect of ponderomotive forces on the nonlinear dynamics of shear Alfvén waves, which manifests itself through high spatial harmonic generation and large amplitude plasma density perturbations. In a finite β plasma these effects can be described in terms of the nonlinear coupling of shear Alfvén waves to slow magnetosonic waves (SMW), and it will be shown that they become especially important when the standing Alfvén waves are driven by an external source. In order to develop an analytical framework for the various processes to be described, we shall consider a simplified model of nonlinear effects in standing shear Alfvén waves in a uniform plasma. Though the derivative nonlinear Schroedinger equation (DNLS) is often used for the study of propagating, large amplitude Alfvén waves [*Mjølhus,* 1976; *Kennel et al.,* 1988], it cannot be applied directly to standing waves and so we have chosen to develop theoretical and computational models by beginning with the full set of MHD equations. Our theoretical models are based on perturbation expansions of the fields while the computer simulations use the full set of nonlinear ideal MHD equations.

It is well known that second-order terms in the ideal MHD equations do not modify the shear Alfvén component of the waves [*Hollweg,* 1971]. The inclusion of second-order terms does, however, lead to strong ponderomotive forces in standing waves in a low β plasma, with secularly growing densities in the region of the maxima in the electric fields of the waves [*Allan,* 1993]. We shall discuss how finite β can inhibit second-order ponderomotive forces through coupling to the SMW. Finite β effects might also play a role in determining the maximum amplitude of FLRs on field lines threading the finite β region of the inner plasma sheet. Figure 1 shows the approximate locations of these FLRs in the equatorial plane (see the examples in the work by *Samson et al.* [1992]). If ionospheric dissipation is not too large, FLRs in the inner edge of the plasma sheet can grow to large enough amplitudes to drive nonlinear instabilities such as the Kelvin-Helmholtz instability in the equatorial plane of the resonances. In particular, *Rankin et al.* [1993b] have shown that with a plasma β of 0.5 and realistic ionospheric conductivities, driven FLRs can grow to amplitudes large enough to allow the nonlinear Kelvin-Helmholtz instability to occur. In the lower β plasma closer to the Earth the results of the present study suggest that ponderomotive forces and the accompanying nonlinear phase shift of the SAWs might lead to earlier saturation of FLRs.

In this paper we shall consider two configurations: the temporal evolution of an initialized, large-amplitude standing Alfvén wave, which we shall refer to as the initial value problem, and the evolution of a standing Alfvén wave excited by a spatially distributed driver.

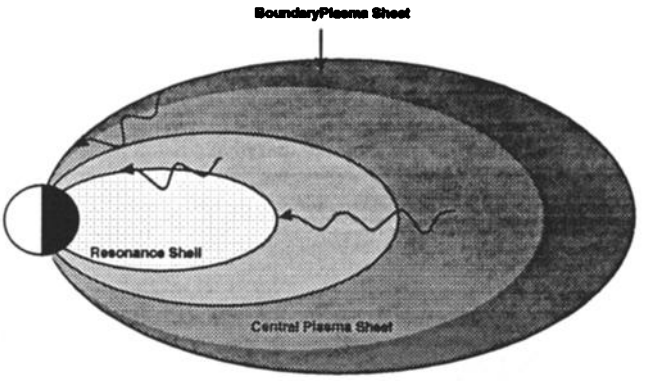

Figure 1. Position of field line resonances in the nightside of the Earth's magnetosphere. Pressure disturbances in the solar wind can couple to high-latitude shear Alfvén resonances at radial distance of approximately $10R_E$ in the equatorial plane.

The latter model is appropriate for the driven FLRs and iononospheric cavity modes discussed above. We also consider the effects of finite β on the two basic configurations, although we defer for future study a detailed discussion of the effects of finite β on the driven system, as well as a consideration of different models for the driver.

2. Ponderomotive Force in the Cold Plasma Limit

In this section we shall consider a magnetohydrodynamic (MHD) model in which the plasma is described using the ideal MHD equations:

$$\begin{aligned} \rho\left(\frac{\partial}{\partial t}+\mathbf{V}\cdot\nabla\right)\mathbf{V} &= -\nabla P+\mathbf{J}\times\mathbf{B}, \\ \nabla\times\mathbf{E} &= -\frac{\partial\mathbf{B}}{\partial t}, \\ \nabla\times\mathbf{B} &= \mu_0\mathbf{J}, \\ \mathbf{E}+\mathbf{V}\times\mathbf{B} &= 0, \\ \frac{\partial\rho}{\partial t}+\nabla\cdot(\rho\mathbf{V}) &= 0. \end{aligned} \tag{1}$$

In the system (1) above, ρ represents the plasma density, $\mathbf{V}$ the fluid velocity, $\mathbf{B}$ the magnetic field, $\mathbf{E}$ the electric field, $\mathbf{J}$ the current density, and P is the pressure in the plasma. It is possible to eliminate the electric field from the system (1) above by using the Ohm's law in the Faraday equation, and correspondingly the current density can be eliminated from the momentum equation using Ampere's law.

In the discussion that follows, we will examine the nonlinear evolution of shear Alfvén waves in the plasma by constructing a perturbation expansion of the fields in (1) of the form, $A = A_0+\epsilon A^{(1)}+\epsilon^2 A^{(2)}+\epsilon^3 A^{(3)}+\ldots$; ϵ is a small expansion parameter that will be proportional to the amplitude of the excited Alfvén wave or driver. It is assumed that the plasma is immersed in a

constant applied magnetic field $\mathbf{B}_0$ directed along the z-axis. For the moment, we consider the situation of a cold homogeneous plasma, $\beta \equiv 2\mu_0 P/B_0^2 \to 0$, in which a shear Alfvén wave is propagating in the x, z plane. This means that only the y-components of the wave magnetic field and velocity are nonzero and in the linear approximation they satisfy the well known MHD wave equations:

$$\frac{\partial B_y^{(1)}}{\partial t} - B_0 \frac{\partial V_y^{(1)}}{\partial z} = 0, \qquad \frac{\partial V_y^{(1)}}{\partial t} - \frac{B_0}{\rho_0 \mu_0} \frac{\partial B_y^{(1)}}{\partial z} = 0. \tag{2}$$

In looking for nonlinear effects within the framework of the ideal MHD equations, it can be shown that such effects are weak for traveling shear Alfvén waves; the existence of standing waves along the field lines produces much stronger nonlinear effects through ponderomotive forces which expel plasma away from maxima in the wave magnetic field intensity. In the magnetosphere, plasma is redistributed along geomagnetic field lines and this effect contributes nonlinear terms to the Alfvén wave equations discussed above.

To show the effect of the ponderomotive force on standing Alfvén waves, we consider a simple case in which the initial fields are represented as sinusoidal plane waves:

$$\begin{aligned} B_y^{(1)} &= B_{y0} = -bB_0 \sin(\omega t - k_x x)\sin(k_z z), \\ V_y^{(1)} &= V_{y0} = bV_A \cos(\omega t - k_x x)\cos(k_z z). \end{aligned} \tag{3}$$

Here $V_A = B_0/\sqrt{\rho_0 \mu_0}$ is the Alfvén velocity, $b \ll 1$ is the dimensionless amplitude, and it can easily be demonstrated that the wave frequency satisfies the dispersion equation for shear Alfvén waves $\omega^2 = k_z^2 V_A^2$. The expressions (3) are exact first-order solutions of the ideal MHD equations, that is, corresponding to the system (2). Proceeding to the evaluation of second order nonlinear terms, it can be determined that the ideal MHD equations can be written in terms of three groups of equations corresponding to the three basic wave modes of the plasma.

The first set corresponds to a shear Alfvén wave with second-order wave amplitudes $B_y^{(2)}$ and $V_y^{(2)}$, which satisfy equations of exactly the same form as the system (2). Therefore this mode is not driven for the case considered here and we can set $B_y^{(2)} = V_y^{(2)} = 0$. This explains perhaps why some authors assume that the shear Alfvén wave fields of the system (3) are proper solutions to the full set of nonlinear ideal MHD equations.

The second set of second-order equations corresponds to the compressional Alfvén mode,

$$\begin{aligned} \frac{\partial V_x^{(2)}}{\partial t} + \frac{B_0}{\rho_0 \mu_0}\left(\frac{\partial B_z^{(2)}}{\partial x} - \frac{\partial B_x^{(2)}}{\partial z}\right) &= -\frac{1}{\rho_0 \mu_0} B_{y0} \frac{\partial B_{y0}}{\partial x}, \\ \frac{\partial B_x^{(2)}}{\partial t} - B_0 \frac{\partial V_x^{(2)}}{\partial z} &= 0, \\ \frac{\partial B_z^{(2)}}{\partial t} + B_0 \frac{\partial V_x^{(2)}}{\partial x} &= 0. \end{aligned} \tag{4}$$

These three equations can be combined into the following form:

$$\frac{\partial^2 V_x^{(2)}}{\partial t^2} - V_A^2 \left(\frac{\partial^2 V_x^{(2)}}{\partial x^2} + \frac{\partial^2 V_x^{(2)}}{\partial z^2}\right) = -\frac{1}{2\rho_0 \mu_0} \frac{\partial^2 B_{y0}^2}{\partial t \partial x} \tag{5}$$

and although the compressional mode is driven by the fields of the incident shear Alfvén wave, it can be shown that the driving terms are not resonant (there is also a resonance with the compressional mode for the special case $k_z = k_x$, but this will not be discussed here) and consequently the coupling between the modes is weak. The solutions to (4), with zero initial conditions, correspond to second-order expressions (proportional to b^2) for constant amplitude field components which oscillate at second harmonic frequencies in space and time. It is easily shown that these components have a negligible feedback effect on the dynamics of the SAW.

The third set of equations corresponds to driven density perturbations (the cold plasma limit of the slow magnetosonic wave),

$$\begin{aligned} \frac{\partial V_z^{(2)}}{\partial t} &= -\frac{1}{2\rho_0 \mu_0} \frac{\partial B_{y0}^2}{\partial z}, \\ \frac{\partial \delta\rho^{(2)}}{\partial t} &= -\rho_0 \left(\frac{\partial V_z^{(2)}}{\partial z} + \frac{\partial V_x^{(2)}}{\partial x}\right) \end{aligned} \tag{6}$$

and as will be shown below, this mode can be resonantly driven by the fields of shear Alfvén waves. An analysis of the equations described above shows that the components $V_z^{(2)}$ and $\delta\rho^{(2)}$ both have secularly growing in time components and therefore provide the dominant nonlinear response of the plasma to shear Alfvén waves. Substituting the expression for B_{y0} in (3) into the system (6), neglecting V_x, and considering only the dominant secular terms, we obtain

$$\begin{aligned} V_z^{(2)} &\cong \frac{-b^2}{4} V_A \omega t \sin(2k_z z), \\ \delta\rho^{(2)} &\cong \frac{b^2}{4} \rho_0 (\omega t)^2 \cos(2k_z z). \end{aligned} \tag{7}$$

It can be verified that it is just standing Alfvén waves that generate this secular response. In the case of oblique traveling waves, there is only an oscillatory $V_z^{(2)}$ component and no density perturbation. Because of their secular temporal behavior, it is expected that effects due to $\delta\rho^{(2)}$ and $V_z^{(2)}$ should dominate the nonlinear behavior of the initial Alfvén wave fields. Therefore, in order to avoid a large amount of unnecessary algebra, we account for only these terms when constructing third order equations describing modifications to the shear Alfvén wave fields (3) which occur on the time scale satisfying $\omega t \gg 1$. The third-order system

$$\begin{aligned} \frac{\partial B_y^{(3)}}{\partial t} - B_0 \frac{\partial V_y^{(3)}}{\partial z} &= -\frac{\partial (V_z^{(2)} B_{y0})}{\partial z}, \\ \frac{\partial V_y^{(3)}}{\partial t} - \frac{B_0}{\rho_0 \mu_0} \frac{\partial B_y^{(3)}}{\partial z} &= -\frac{\delta\rho^{(2)} B_0}{\rho_0^2 \mu_0} \frac{\partial B_{y0}}{\partial z} - V_z^{(2)} \frac{\partial V_{y0}}{\partial z} \end{aligned} \tag{8}$$

is identical to the system (2) with the exception of the nonlinear driving terms appearing on the right-hand side of the equations; these are related to the secularly growing plasma density perturbations. Substitution of the expressions (7) and (3) into the nonlinear system (8) reveals two major nonlinear effects on the initial Alfvén wave: higher harmonic generation and a frequency shift of the fundamental wave. Indeed, according to (8) the interaction of the Alfvén wave (3) with the density perturbation (7) produces additional terms which correspond to oscillations in B_y at wave numbers $(k_x, 3k_z)$ and frequency ω. These terms do not satisfy the linear dispersion equation for the shear Alfvén wave, and therefore they grow with time like $(\omega t)^2$, that is, at the same rate as the density perturbations in (7) which drive them:

$$\delta B_y^{(3)} \cong \frac{3}{64} B_0 b^3 (\omega t)^2 \sin(\omega t - k_x x)\sin(3k_z z),$$
$$\delta V_y^{(3)} \cong -\frac{1}{64} V_A b^3 (\omega t)^2 \cos(\omega t - k_x x)\cos(3k_z z). \quad (9)$$

The nonlinear terms in (8) also produce corrections to the shear Alfvén wave which correspond to oscillations at wave numbers (k_x, k_z) and frequency ω and these have a strong effect on the initial shear Alfvén fields because they satisfy the linear shear Alfvén wave dispersion equation. Adding these corrections to the initial fields of the system (3), we obtain equations describing modifications to the shear Alfvén waves,

$$B_y \cong -bB_0\left(1 - \frac{b^2}{32}(\omega t)^2\right)\sin(\omega t - k_x x)\sin(k_z z) + \frac{b^3}{48} B_0 (\omega t)^3 \cos(\omega t - k_x x)\sin(k_z z),$$
$$V_y \cong +bV_A\left(1 - \frac{3b^2}{32}(\omega t)^2\right)\cos(\omega t - k_x x)\cos(k_z z) + \frac{b^3}{48} V_A (\omega t)^3 \sin(\omega t - k_x x)\cos(k_z z). \quad (10)$$

The first term on the right-hand side of the above equations describes the decrease in amplitude of the initial fields of the shear Alfvén wave. It can also be seen that the dominant terms in (10) grow like t^3, and that they produce a shift in the frequency of the shear Alfvén wave. Comparison of the dominant nonlinear terms in (10) with the initial linear terms shows that the perturbational approach fails at a time given by

$$\omega t_{NL} = (48)^{1/3} b^{-2/3} \quad (11)$$

when all other nonlinear terms are still relatively small. We can therefore consider t_{NL} as a characteristic time for which strong nonlinear effects are to be expected. For example, with $b = 1\%$, the nonlinear time corresponds to 12 wave periods, whereas with $b = 10\%$ the timescale is less than 3 wave periods. The dominant secular term in (10) for B_y is changing the phase of the initial field from $\sin(\omega t - k_x x)$ to $\cos(\omega t - k_x x)$ and therefore we can interpret this effect as a nonlinear phase shift. Indeed, (10) can be rewritten as

$$B_y \cong -bB_0\left(1 - \frac{b^2}{32}\omega^2 t^2\right)\sin(\omega t - k_x x + \phi)\sin(k_z z),$$
$$V_y \cong bV_A\left(1 - \frac{3b^2}{32}\omega^2 t^2\right)\cos(\omega t - k_x x + \phi)\cos(k_z z),$$
$$\phi(t) = -\operatorname{asin}\left(\frac{b^2}{48}\omega^3 t^3\right). \quad (12)$$

In the small time limit the phase shift can be approximated by

$$\phi(t) \approx -b^2(\omega t)^3/48 \quad (13)$$

and it can be seen that the temporally growing phase ϕ results in a negative frequency shift of the fundamental Alfvén wave of the form,

$$\delta\omega = \frac{d\phi(t)}{dt} = -\frac{b^2}{16}\omega^3 t^2. \quad (14)$$

Strictly speaking, (13) is valid only for $\phi(t) \ll 1$ but the numerical results to be discussed later indicate a much broader region of validity. One can see that at the nonlinear time given by (11) the relative frequency shift and amplitude variation are of the order of $b^{2/3}$ and therefore are small compared to the initial values (the frequency shifts are still experimentally observable; for example, $\delta\omega/\omega \approx 0.04$ for $b = 1\%$, $\delta\omega/\omega \approx 0.18$ for $b = 10\%$). Correspondingly, at the time $t = t_{NL}$, the magnitude of the density perturbations is also small,that is, they are also of order $b^{2/3}$.

The temporal behavior for $t > t_{NL}$ depends strongly on the plasma parameters. As will be shown later, numerical simulations of the full MHD equations demonstrate that in the case of cold plasmas the absence of thermal pressure fails to prevent the contraction of plasma into the nodes of the Alfvén wave magnetic field. Therefore the density inhomogeneities grow to very large amplitudes ($\delta\rho \gtrsim \rho_0$) and totally destroy the initial periodic Alfvén wave. Presumably, kinetic effects such as wave breaking can come into play in such a situation. However, the inclusion of finite temperature may have a dramatic effect on the nonlinear evolution, even in the case of small β. It will be shown in section 4 that in this case the secular behavior of the density perturbations is inhibited due to the slow reaction of the plasma to the thermal pressure force.

3. Temporal Evolution of Driven Shear Alfvén Waves

In the Earth's magnetosphere, large-amplitude shear Alfvén waves presumably do not exist as initial conditions under normal magnetospheric conditions but are more likely to be driven by some external source. In particular, it is well known that global magnetospheric resonance modes [*Allan and Poulter*, 1989], which are trapped compressional Alfvén waves in an inhomogeneous plasma, experience collisionless damping when they encounter a local resonance with shear Alfvén waves. From the point of view of the fields of shear Alfvén waves, the global resonances constitute an external driving force that can be represented by a specified source in our model equations describing coupling between SAWs and density perturbations in a homogeneous plasma. Formally, this driving force can be

represented through the addition of the terms

$$-\omega_0 RB_0 \sin(\omega_0 t - k_x x)\sin(k_z z),$$
$$\omega_0 RV_A \cos(\omega_0 t - k_x x)\cos(k_z z) \quad (15)$$

to the right-hand sides of the equations for B_y and V_y, respectively, of the first-order system (2). In this case the dimensionless parameter R describes the relative strength of the driver. For example, in the case of shear Alfvén waves excited by a compressional driver, $R \approx \delta P / P_0$ where δP is the amplitude of the pressure wave. The solutions to the driven linear equations can be written as,

$$B_{yd} = -\omega_0 RB_0 t \sin(\omega_0 t - k_x x)\sin(k_z z),$$
$$V_{yd} = \omega_0 RV_A t \cos(\omega_0 t - k_x x)\cos(k_z z). \quad (16)$$

It can be seen that the system (16) describes linear growth of the fields of the shear Alfvén waves due to the external driver. This situation is in accord with a field line resonance which is being driven to large amplitude by a global excitation source. To proceed, we repeat the calculation of section 2 in which we determined the dominant secular terms driving the density and field-aligned velocity component associated with the density perturbations. In the second-order approximation we again account for only the fastest growing components of $V_z^{(2)}$ and $\delta\rho^{(2)}$. Under the same assumptions as before we solve (6) with the source term B_{y0} replaced by B_{yd} of system (16). The solution for $V_z^{(2)}$ can be written as

$$\begin{aligned} V_z^{(2)} = & \\ & -\frac{1}{12}V_A R^2(\omega_0 t)^3 \sin(2k_z z) \\ & -\frac{1}{16}V_A R^2 \sin(2k_z z)\sin(2k_x x) \\ & +\frac{1}{8}V_A R^2 \omega_0 t \sin(2k_z z)\cos(2\omega_0 t - 2k_x x) \\ & -\frac{1}{8}\left(\frac{1}{2} - (\omega_0 t)^2\right)V_A R^2 \sin(2k_z z)\sin(2\omega_0 t - 2k_x x). \end{aligned} \quad (17)$$

Note that along with the fastest growing term t^3 in the above equation, which is similar to the secular term in (7), there are also smaller amplitude second harmonic components in the x direction. In similar fashion it can also be shown that the compressional component $V_x^{(2)}$ has nonresonant terms with wave numbers $(2k_x, 0)$ and $(2k_x, 2k_z)$, respectively, and with corresponding frequencies $2k_x V_A$ and $2\sqrt{k_x^2 + k_z^2}V_A$. The relative amplitudes of these terms are proportional to R^2, and since their growth is proportional to t^2, which is slower than for $V_z^{(2)}$, they can again be neglected. Therefore, in the case where shear Alfvén waves are driven by an external source, the dominant secular behavior can be described using the equations,

$$V_z^{(2)} = -\frac{1}{12}V_A R^2(\omega_0 t)^3 \sin(2k_z z),$$
$$\delta\rho^{(2)} = \frac{1}{24}\rho_0 R^2(\omega_0 t)^4 \cos(2k_z z). \quad (18)$$

The long-term effect of the second-order density perturbations on the fields of the main harmonic driven shear Alfvén wave may again be expressed using (8). On substituting (18) and (15) into the right-hand sides of the third-order system (8), and solving the resulting equations for $V_y^{(3)}$, we obtain,

$$\begin{aligned} V_y = & V_A(R\omega_0 t)\left(1 - \frac{1}{64}R^2\omega_0^4 t^4\right)\cos(k_z z)\cos(\omega_0 t - k_x x) \\ & + \frac{1}{576}V_A(R\omega_0 t)R^2\omega_0^5 t^5 \cos(k_z z)\sin(\omega_0 t - k_x x) \\ & + \frac{1}{384}V_A(R\omega_0 t)R^2\omega_0^4 t^4 \cos(3k_z z)\cos(\omega_0 t - k_x x) \end{aligned} \quad (19)$$

where we have added the third-order terms to the fields of the main harmonic wave. In (19) we have also included the third spatial harmonic term $(k_x, 3k_z)$ corresponding to (9) in the undriven case. It can be seen that the form of (19) is similar to (10) if we replace the parameter b in the former by $R\omega_0 t$. Only the numerical coefficients are different and it is expected that very similar behavior will therefore occur. The first effect that can be considered is an apparent slowing of the growth of the driven shear Alfvén wave due to the interaction between the driver fields and the ponderomotive density perturbations. The effective amplitude of the driver is now given by

$$b_{NL} = R\omega_0 t\left(1 - \frac{1}{64}R^2\omega_0^4 t^4\right) \quad (20)$$

and the phase shift between the specified driver, (16), and the main harmonic fields now results in a frequency shift given by

$$\frac{\delta\omega}{\omega_0} = -\frac{5}{576}R^2\omega_0^4 t^4. \quad (21)$$

From (19) it may be concluded that when the coefficient multiplying the term $\sin(\omega_0 t - k_x x)$ is comparable to the amplitude of the driver, $R\omega_0 t$, the latter will be out of phase with the driver. When this occurs, it is expected that the main harmonic field V_y will saturate. This defines a saturation timescale for driven shear Alfvén waves of the form

$$t_{NL} \approx 3.5\omega_0^{-1}R^{-2/5}. \quad (22)$$

At the nonlinear timescale given by (22) the amplitude of the excited SAW corresponds to

$$b_{NL} = R\omega_0 t_{NL} \approx 3.5R^{3/5}. \quad (23)$$

Notice that at the time of saturation the nonlinear corrections to the effective wave amplitude given by (20) are still small. They are of the order of $R^{2/5}$, which is much smaller than unity.

It may be concluded that the main differences between the driven and initial value (undriven) problem is that in the latter case nonlinear processes decrease the amplitude of the shear Alfvén waves and produce a continuous frequency shift of the wave. In the driven case, nonlinear effects have a more rapid secular dependence, and in addition the nonlinear frequency shift

of the main harmonic fields can lead to a decoupling between the wave fields and the source. The latter result leads us to conclude that saturation of the fields of the shear Alfvén waves should occur at a timescale determined by (22). However, the effect of nonlinear saturation is out of the limits of applicability of the perturbative approach used in this paper, and the verification of this result must be deduced from numerical solutions to the full set of nonlinear equations. As will be shown later, when we discuss solutions to the full set of nonlinear MHD equations, the saturation timescale in the driven case can be as short as a few wave periods and the wave amplitude of the excited shear Alfvén wave no longer shows significant growth after the time (22).

4. Effect of Finite β on Nonlinear Standing Alfvén Waves

The analysis presented in sections 2 and 3 shows that the components V_x, B_x, and B_z do not exhibit secular behavior and therefore the main nonlinear effects are due to longitudinal plasma motion, which can be described using equations for $V_z^{(2)}$ and $\delta\rho^{(2)}$. In order to account for the effects of finite temperature, it is sufficient to consider only the z-component of the equation of motion, in which the term $-\rho_0^{-1}\partial\delta P/\partial z$ must be added to the right hand side of the first equation in the system (6). Assuming the standard relation $\delta P/\delta\rho = C_S^2$, where C_S is the ion acoustic velocity, we can express (6) in the form of a second order differential equation which describes slow magnetosonic waves (SMW) driven by the ponderomotive force:

$$\frac{\partial^2\delta\rho}{\partial t^2} - C_S^2\frac{\partial^2\delta\rho}{\partial z^2} = \frac{\partial^2}{\partial z^2}\frac{\langle B_y^2\rangle}{2\mu_0}. \qquad (24)$$

The angular brackets in (24) refer to the time averaging of the shear Alfvén wave intensity over its period $2\pi/\omega$. This is appropriate because we are assuming here that $\beta \ll 1$ and therefore the acoustic velocity C_S is much less than V_A.

To evaluate qualitatively the effect of plasma pressure on the nonlinear behavior of shear Alfvén waves, we again make use of the perturbational approach discussed earlier and substitute into the right hand side of (24) the field of an initial undisturbed shear Alfvén wave of the form of (3). The solution of (24) with zero initial conditions corresponds to a driven acoustic wave whose frequency is $\Omega = 2k_zC_S$,

$$\frac{\delta\rho}{\rho_0} = \frac{b^2}{2}\frac{\omega^2}{\Omega^2}[1-\cos(\Omega t)]\cos(2k_z z). \qquad (25)$$

In the limit of a cold plasma, $C_S \to 0$, this expression recovers the previous one, (7), and it can be seen that secular growth corresponds in fact to the initial stage of excitation of a standing SMW with an amplitude $\sim \frac{1}{2}b^2/\beta\gamma$, where γ is the ratio of specific heats. We can conclude therefore that the small amplitude expansion approach should be valid for all times provided $b < \sqrt{2\beta\gamma}$, in order that the relative amplitude of the density perturbations remains small. In that case, (25) shows that finite plasma pressure prevents the formation of strong density perturbations and higher harmonic generation. Equation (25) corresponds to periodic density pulsations that are related to a standing SMW that is driven through nonlinear coupling to shear Alfvén waves. The amplitude of these pulsations will be a decreasing function of time if Landau damping of the slow mode is accounted for. This is especially important if the ions and electrons have comparable temperatures. However, we consider here a nonresonant SMW driven by the ponderomotive force and therefore Landau damping should not change qualitatively the estimate of the density perturbations given by (25) because the damping coefficient is presumably less than the SMW frequency and, in particular, our results indicate that strong nonlinear effects can occur within a fraction of an acoustic wave period provided β is sufficiently small.

From (25) we can distinguish two qualitatively different regimes for the nonlinear evolution of standing SAWs which depend upon the relationship between the wave amplitude and the plasma pressure. The case corresponding to relatively cold plasma, $\beta < b^2$, results in strongly nonlinear behavior: after the time $t \approx \omega^{-1}b^{-1}$, large-amplitude density perturbations ($\delta\rho > \rho_0$) are produced, and it is expected that many odd shear Alfvén wave harmonics will be generated. Presumably, these features manifest themselves through wave breaking and a resulting dissipation of the Alfvén wave energy by plasma particles. The regime corresponding to warm plasma, for which $\beta > b^2$, is quite different. It corresponds to much smoother periodic nonlinear behavior of SAWs. These periodic pulsations will ultimately be damped out and a constant nonlinear frequency shift of the SAW will result.

The same separation between strongly nonlinear nonperiodic behavior, and mildly nonlinear periodic behavior, can be translated onto the driven case if we notice the relation (23) between the saturated amplitude and the strength of the driver. We can expect strongly nonlinear plasma evolution, and large amplitude density perturbations if $R > (\gamma\beta/2)^{5/6}$. This regime will be discussed in the next section when we consider numerical solutions to the full set of MHD equations. Quasi-periodic behavior of SAWs is expected in the case of a warm plasma for which $\gamma\beta/2 > R^{6/5}$. This parameter range needs a more detailed analysis than can be presented here, because the density perturbations associated with SMWs will affect the energy exchange between the excited SAWs and the driving source.

5. Numerical Results and Discussion

In order to test the validity of some of the results presented in sections 2, 3 and 4 above and investigate the long-term evolution of nonlinear SAWs, we will now consider numerical solutions to the full set of nonlinear ideal MHD equations described by the system (1).

The algorithm and numerical techniques that are used to solve (1) are described in the papers by *Rankin et al.* [1993a, b]. We only note here that the ideal MHD equations are finite differenced for a Cartesian geometry, with the assumption of straight magnetic field lines in the z direction. We will first of all describe results obtained for $\beta = 0$, corresponding to the initial value problem. Then we consider the situation in which the shear Alfvén wave field is driven by an external source. Finally, we investigate the effects of finite β on the initial value problem.

The first simulation that we consider corresponds to the initial value problem in which a shear Alfvén wave field is imposed on the system. Periodic boundary conditions are used in the x direction, which corresponds to the propagating direction of the wave, and the fields are chosen to form a standing wave pattern along the z direction, in accordance with (3). The amplitude of the B_y component of the initial wave field corresponds to ten percent of the ambient magnetic field, and the plasma is cold, $\beta = 0$. Figure 2 shows the evolution of the density in the plasma. Initially, the density is uniform and after some time it can be seen that the ponderomotive force causes plasma to accumulate in the valley's of the wave magnetic field intensity B_y^2. The density accumulates to very large amplitude, and the behavior for $\delta\rho/\rho_0 > 1$ presumably signifies the end of the validity of ideal MHD for this cold plasma case. It is readily verified that the above process conserves energy exactly, and thus the saturated amplitude of the density perturbations must be related to effects occurring outside of ideal MHD.

In Figure 3 we show the spatial Fourier transform of the density. At the time indicated in Figure 3a the ponderomotively driven second harmonic density perturbation is dominant. However, at later times, Figure 3b indicates that a large number of even numbered spatial harmonics $2nk_z$ are generated, corresponding to a highly nonlinear stage of evolution of the initial shear Alfvén wave field. The high harmonics in Figure 3 correspond to the excitation of large-amplitude density perturbations which form standing waves along the field lines.

The theory of section 2 deals with the second harmonic density perturbation, and we can therefore expect a comparison of the numerical results and theory to agree only during the early stage of evolution of the waves. Such a comparison is made in Figure 4b, which shows the growth of the $(0, 2k_z)$ component of the density with time. The dashed line corresponds to the analytic expression of (7) and the solid line corresponds to the numerical results. It can be seen that the agreement between the theory and numerical results is excellent, and only at later times does the growth of the $(0, 2k_z)$ harmonic start to slow as a result of higher spatial harmonics being excited. Figure 4a shows the numerical results over the full time simulated. There is evidence of a tendency of the second harmonic to begin saturating, but the validity of the ideal MHD equations is questionable at this stage because the density perturbations are of order one and the corresponding density gradients are very steep.

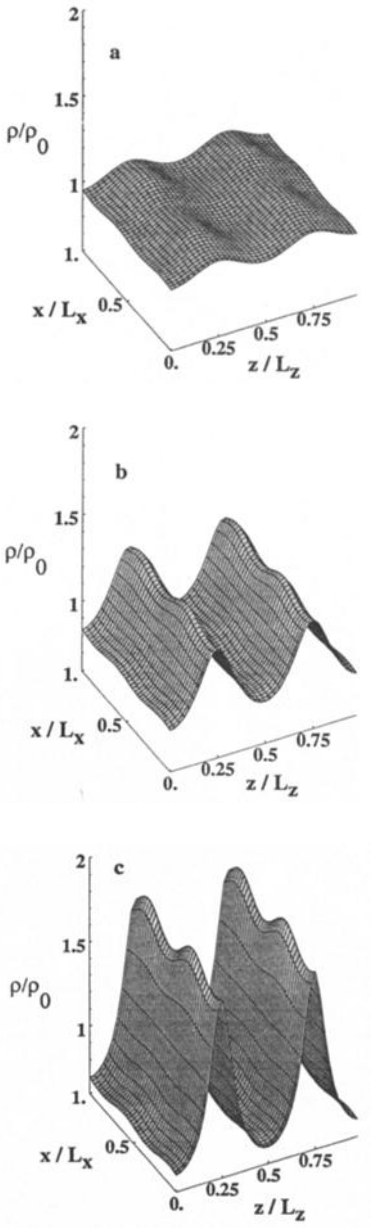

Figure 2. Temporal evolution of density perturbations driven by the ponderomotive force in the initial value problem. The data are shown at three times: (a) $t = 0.67t_{saw}$, (b) $t = 1.40t_{saw}$, (c) $t = 2.13t_{saw}$. The time unit t_{saw} corresponds to the period of the shear Alfvén wave (SAW.)

An inspection of the time dependence of the higher spatial harmonics in the density shows that they grow very precisely like $t^{\frac{1}{2}n+1}$, where n is even. This time dependence corresponds to a cascade process in which subsequent harmonics are produced mainly through beating between the fundamental wave and the previously generated harmonic. The growth of high harmonics to finite amplitude appears delayed because the coupling is initially very weak. After they have grown to finite amplitude their growth is extremely rapid, reflecting the highly nonlinear coupling that is taking place at that stage.

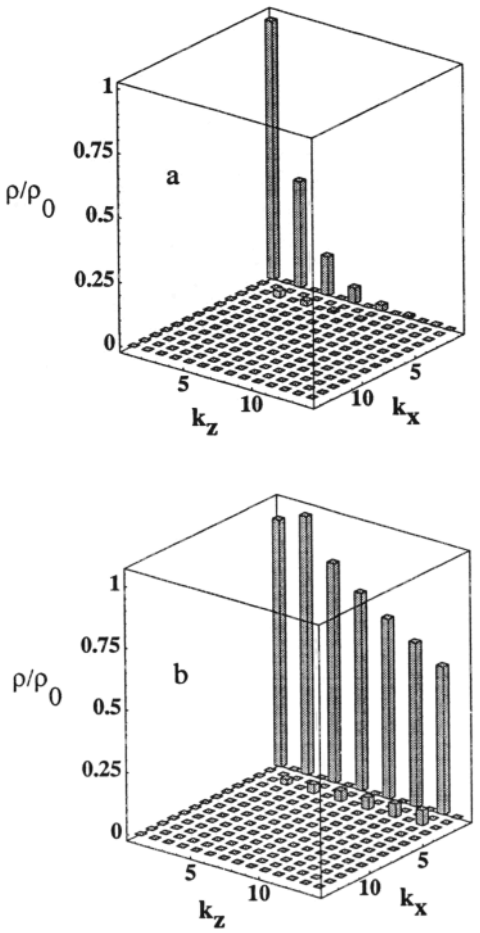

Figure 3. Spatial Fourier transform of the density at a time corresponding to (a) $t = 2.13t_{saw}$, (b) $t = 3.94t_{saw}$. The figure shows a large number of even spatial harmonics $2nk_z$, corresponding to the excitation of large-amplitude density perturbations.

The temporal behavior of the amplitude of the main harmonic shear Alfvén wave is shown in Figure 5. It can be seen that the effect on the main harmonic fields is not too severe. In particular, according to (11), for $b = 0.1$ the timescale for strong nonlinear effects to become important corresponds to $t_{NL} \approx 1.5t_{saw}$, where $t_{saw} = 2\pi/\omega$ is the period of the SAWs. At this time, the amplitude depletion of the initial fields is roughly 10%, even though large-amplitude fluctuations in the density are being produced.

The next effect that can be investigated is the phase change of the main harmonic field due to beating between the ponderomotive density perturbations and the incident wave field. Figure 6 shows a comparison between the analytic expression (the third equation in the system (12)), its small time limit, (13), and the numerical results. The lower curve in Figure 6 is the analytic result (12) and indicates that saturation should occur when the phase shift is $\pi/2$. This is all that can be expected of the perturbation theory used here. The upper curve corresponds to the analytic expression in the small time limit, (13), and it can be seen that it agrees with the numerical results (the middle curve) well beyond its strict region of validity. This behavior is common in perturbation treatments of nonlinear systems. The differences between the analytic and numerical results become important at timescales for which high harmonics are generated. It can be seen from Figure 6 that the agreement with the theory is initially very good. For the time interval over which growth is shown, the phase shift of the initial wave field is greater than π. To investigate the longer time behavior of the system a nonperturbative treatment must be used and this is currently under investigation. However, from Figure 6 it can be deduced that at later times the frequency shift demonstrates a tendency toward stabilization.

Having established the validity of the analytic results presented in section 2, we will now move on and consider the situation in which the shear Alfvén wave field is driven by an external source. To model this in the simulations, we apply an excitation field of the form of (15) at each point on the finite difference simulation grid. The main effect that we are interested in studying is the possible saturation of the linearly growing excited shear Alfvén waves due to dephasing from the externally applied driver. This effect is directly related to field line resonances driven by global compressional

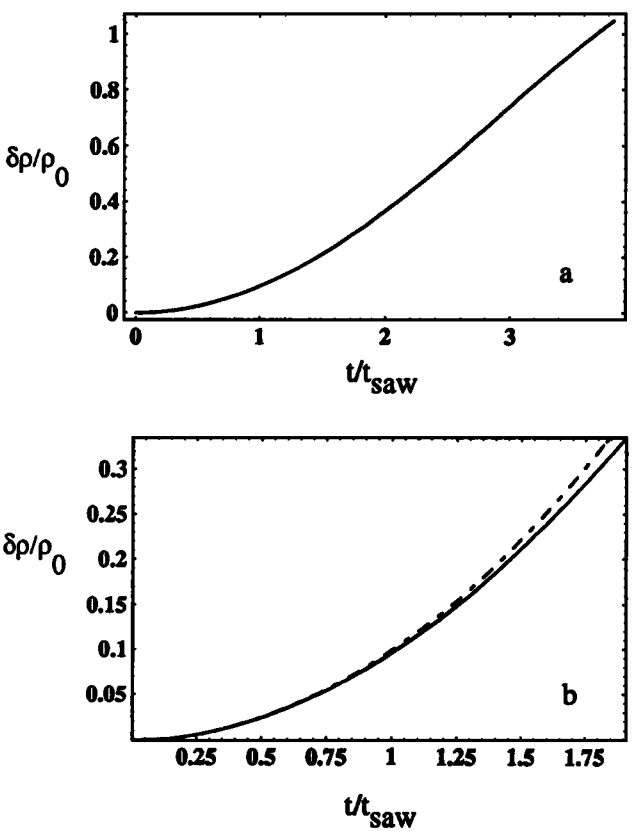

Figure 4. Temporal evolution of the amplitude of the $(k_z = 0, 2k_z)$ spatial harmonic in density. (a) Numerical results are shown; (b) the dashed line is the theoretical result, and the solid line corresponds to the numerical results. The time unit t_{saw} corresponds to the period of the SAW.

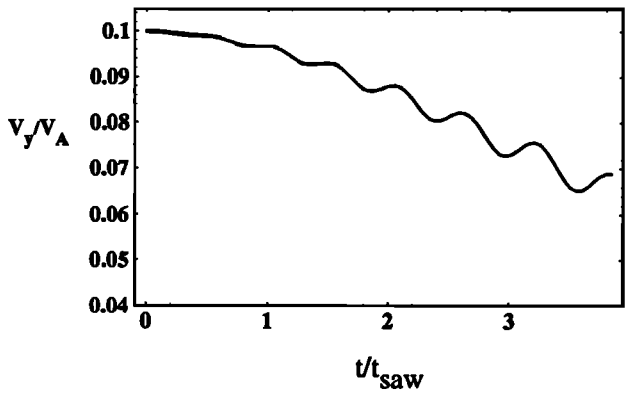

Figure 5. Temporal evolution of the amplitude of the main harmonic shear Alfvén wave field. The amplitude starts to deplete when high harmonics are generated. The time unit t_{saw} corresponds to the period of the SAW.

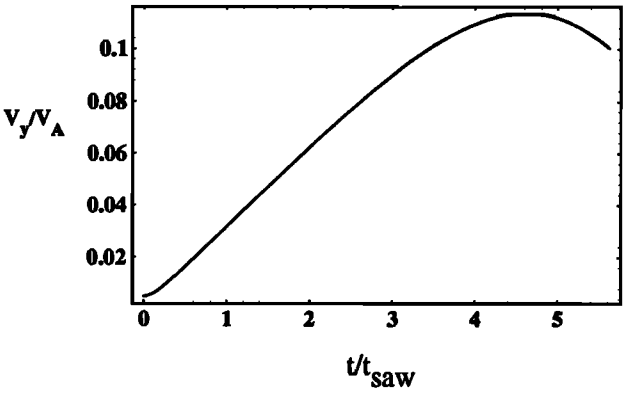

Figure 7. Temporal growth of V_y corresponding to the main harmonic shear Alfvén wave field for the driven case. The fields initially grow linearly with time and saturate at later times due to dephasing from the externally applied driver. The time unit t_{saw} corresponds to the period of the SAW.

magnetospheric waves and may also be related to large-amplitude shear Alfvén waves formed in the cavity between the ionosphere and the high-altitude peak in the Alfvén velocity profile.

In the driven case we have confirmed the analytic estimates of the rates of growth of the $(0, 2k_z)$ spatial harmonic density perturbation and have verified the frequency shift of the fundamental wave as determined by (18) and (21) above. For the simulation described below we impose a driver with an amplitude corresponding to $R = 0.005$ in (15). The evolution with time of the V_y component of the excited shear Alfvén wave field is shown in Figure 7. The initial stage corresponds to linear growth with time in accord with expression (16) above. Thereafter, dephasing accumulates at a rate which is large enough to slow the growth of the excited wave. At the time of saturation in Figure 7, the phase shift from the driver is $\pi/2$, and the driver is essentially decoupled from the excited wave fields. It is interesting to compare the saturation timescale in the simulations with the analytic result given by (22). On substituting the value $R = 0.005$ into expression (22) we estimate a saturation time corresponding to approximately four periods of the shear Alfvén driver fields. This value compares well to the saturation time observed in the simulations. The saturated amplitude also compares well to the analytic estimate given by Eq. (23). A direct comparison of the numerical results with the estimate in (22) is valid provided that high spatial harmonics are not excited. However, at the late stages in Figure 7 the wave fields are highly nonlinear, and the agreement with the theory is therefore rather gratifying.

In the driven case, (19) also indicates that there should be a secularly growing third spatial harmonic component $(k_z, 3k_z)$ of the SAW field. Figure 8 compares the predicted analytic growth of this component with the results of the simulations. From (19) the $(k_z, 3k_z)$ driven component of the SAW grows rapidly

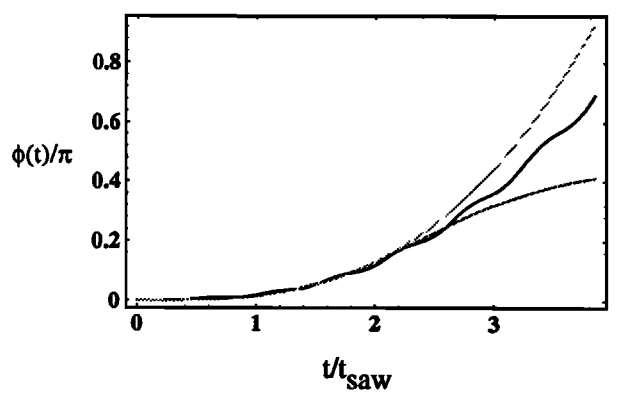

Figure 6. Temporal evolution of the phase of the main harmonic shear Alfvén wave field. The lower curve is the analytic phase shift of (12). The upper curve is the small time limit phase shift, (13), and the middle curve indicates the numerical result. The small time limit phase shift follows the numerical results well beyond its region of validity. The time unit t_{saw} corresponds to the period of the SAW.

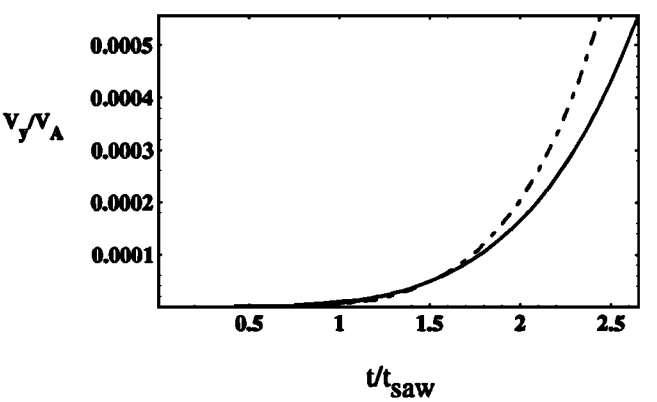

Figure 8. Temporal growth of the nonlinear $(k_z, 3k_z)$ third spatial harmonic component of the SAW for the driven case. The dashed line is the theoretical result, and the solid line corresponds to the numerical results. The time unit t_{saw} corresponds to the period of the SAW.

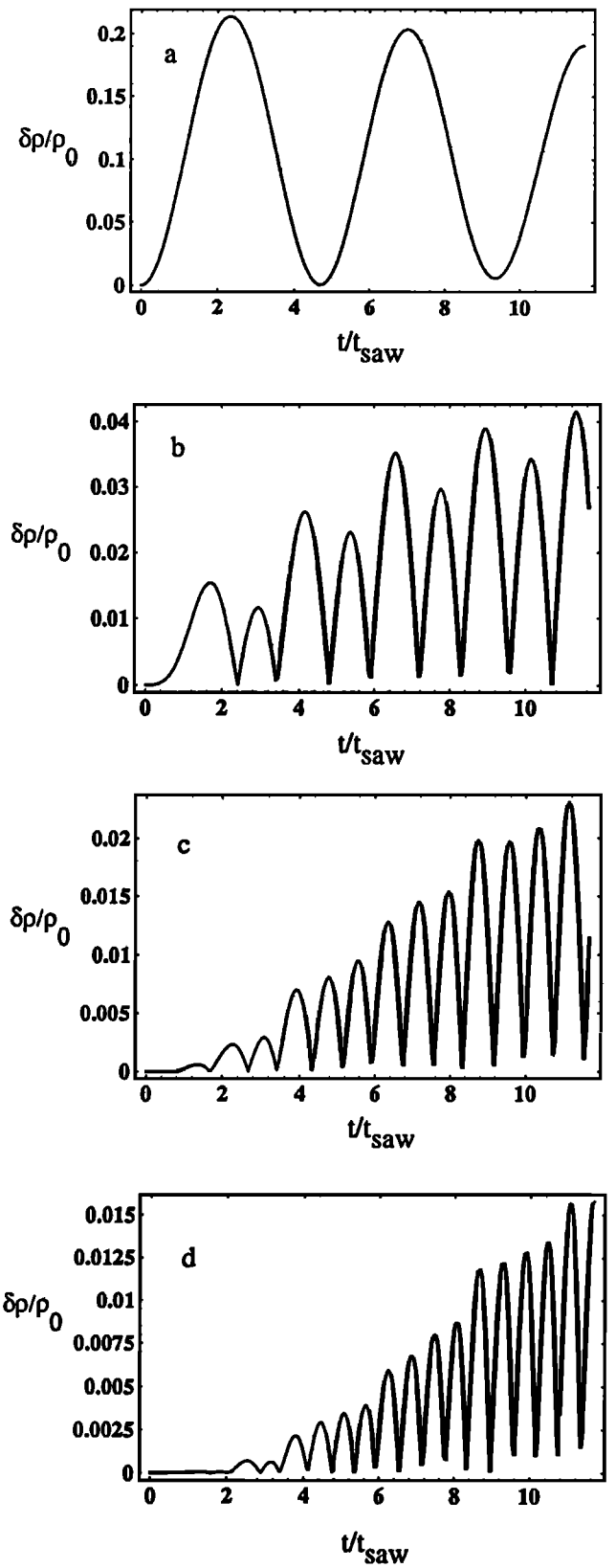

Figure 9. Temporal evolution of the amplitudes of $(0, 2nk_z)$ spatial harmonics in the density for a finite temperature plasma, $\beta = 0.013$, corresponding to the excitation of SMWs; (a) n=1, (b) n=2, (c) n=3, (d) n=4. The time unit t_{saw} corresponds to the period of the SAW. Note the initial time delays before harmonics have had time to grow and the different scale of the amplitudes of the harmonics.

with time like R^3t^5, and this is the dependence that can be seen in Figure 8. However, the coefficients multiplying the secular term in (19) are small, and thus the effects of this wave are negligible.

The final situation that we consider corresponds to the case where the plasma has a finite temperature. For example, in Figure 9 we show the temporal evolution of the $2nk_z$ spatial harmonics of the SMW for the range $n = 1$ to $n = 4$. According to the discussion of section 4, the second spatial harmonic of the SMW should saturate at an amplitude $\frac{1}{2}b^2/\beta\gamma$. Taking $b = 0.1$, and $\beta = 0.013$, the saturation amplitude according to this formula corresponds to $\delta\rho/\rho_0 = 0.23$. Comparing this estimate to the maximum amplitude of the $2k_z$ SMW in Figure 9, it can be seen that saturation occurs at a value that is close to the theoretical prediction. The higher spatial harmonics in Figure 9 begin to saturate at much smaller amplitudes than the $(0, 2k_z)$ slow mode, and thus in a warm plasma coupling to the fundamental slow mode component provides the dominant nonlinear behavior. Note that in contrast to the spatial harmonics of the SAW the frequencies of higher magnetosonic harmonics grow in proportion to their wave number, as is expected for the case of impulse excitation.

6. Conclusions

The theory and numerical simulations presented above suggest that nonlinear effects on standing shear Alfvén waves can be very strong in a low β plasma regime, which in the present study is appropriate for ionospheric cavity modes and for FLRs excited in the vicinity of the central plasma sheet. It has been shown that the ponderomotive force can lead to high harmonic generation, secularly growing frequency shifts of the fundamental waves, and in the case of driven systems, can result in nonlinear saturation and dephasing of driven shear Alfvén wave fields. In the driven case, one important aspect of the estimates of saturation is that nonlinear effects can take place on a timescale of the order of a few wave periods, when large ponderomotive density enhancements occur. These timescales are compatible with observations [*Samson et al.*, 1992] of large-amplitude field line resonances in the Earth's magnetosphere, which indicate that the wave packets that are responsible for exciting the waves have durations of only a few wave cycles.

Processes which determine the saturation amplitudes of field line resonances include Joule heating losses at the ionosphere and nonlinear processes such as the Kelvin-Helmholtz instability [*Rankin et al.*,1993a] and the tearing mode instability [*Seyler*, 1990]. The results of the present work suggest that the ponderomotive force should be added to the list of possible saturation mechanisms. In order to demonstrate this fact we have repeated the simulation of field line resonances reported by *Rankin et al.* [1993b], in which a large-amplitude shear Alfvén resonance was excited by a compressional mode driver in a plasma with $\beta = 0.5$ (see, for example, *Rankin et al.*,1993b, Figure 5). The simulation

was rerun for the cold plasma case, and it was found that nonlinear harmonic generation prevented the field line resonance from growing to large amplitude. Thus harmonic generation may constitute an effective saturation mechanism if the plasma is sufficiently cold. The FLRs observed by *Samson et al.* [1992] are seen only at high latitudes on field lines threading the inner edge of the plasma sheet, particularly during substorm growth phases. *Pu et al.* [1992] have also shown that β can be greater than one at geosynchronous orbit at the time of substorm onset. Thus the observed FLRs are excited in a region of high β, where according to the theory presented above harmonic generation is unlikely to provide a mechanism for strong nonlinear saturation. Outside of this high β plasma, excited FLRs should saturate at relatively low amplitudes and this may explain why certain FLRs are consistently observed over a narrow range of latitudes. A more detailed analysis of ponderomotive effects on driven field line resonances at finite β is currently under investigation.

The theory of sections 2 and 3 is also relevant to observations of large amplitude shear Alfvén waves in the high-latitude Alfvén wave resonator, for which the condition $\beta \ll 1$ is satisfied. In such circumstances we can expect strong nonlinear saturation of shear Alfvén waves, together with strong density perturbations and the accumulation of plasma in the vicinity of minima in the wave magnetic field. Ion acceleration along the magnetic field lines should also accompany this process [cf. *Li and Temerin*, 1993; *Allan*, 1993]. This acceleration should occur over small distances of the order of a fraction of a wavelength, in the region where ponderomotive density accumulation takes place (i.e., at the B_y field minima). Because of the secular nature of the field-aligned velocity component, it is expected that the accelerated ions will form a pulse in which different ion species will have approximately the same velocity but will have different energies due to their different masses ($\epsilon_i = \frac{1}{4} m_i \langle V_y^2 \rangle$). A more accurate analysis of ion acceleration must take into account geometrical effects, the temporal behavior of SAWs in the nonlinear regime, and the effect of inhomogeneity in the ambient plasma. This will be addressed in a future work.

Acknowledgments. This research was supported by the Natural Sciences and Engineering Research Council of Canada (NSERC) and in part by the Russian Foundation of Fundamental Investigations.

The Editor thanks R.L. Lysak and M.A. Temerin for their assistance in evaluating this paper.

References

Allan, W., Plasma energization by the ponderomotive force of magnetospheric standing Alfvén waves, *J. Geophys. Res.*, *98*, 11,383, 1993.

Allan, W., and E. M. Poulter, Damping of magnetospheric cavity modes: A discussion, *J. Geophys. Res.*, *94*, 11,843, 1989.

Barnes, A., and J. V. Hollweg, Large amplitude hydromagnetic waves, *J. Geophys. Res.*, *79*, 2302, 1974.

Belcher, J. W., and L. Davis Jr., Large amplitude Alfvén waves in the interplanetary medium, *J. Geophys. Res.*, *76*, 3534, 1971.

Boehm, M. H., C. W. Carlson, J. P. McFadden, J. H. Clemmons, and F. S. Mozer, High resolution sounding rocket observations of large amplitude Alfvén waves, *J. Geophys. Res.*, *95*, 12,157, 1990.

Cohen, R. H., and R. M. Kulsrud, Nonlinear evolution of parallel propagating hydromagnetic waves, *Phys. Fluids*, *17*, 2215, 1975.

Granik, A. T., Large-amplitude waves in an anisotropic plasma, *J. Geophys. Res.*, *86*, 5431, 1981.

Hollweg, J. V., Density fluctuations driven by Alfvén waves, *J. Geophys. Res.*, *76*, 5155, 1971.

Kennel, C. F., B. Buti, T. Hada, and R. Pellat, Nonlinear, dispersive, elliptically polarized Alfvén waves, *Phys. Fluids*, *31*, 1949, 1988.

Lashmore-Davies, C. N., Modulational instability of a finite amplitude Alfvén wave, *Phys. Fluids*, *19*, 587, 1976.

Li, X., and M. Temerin, Ponderomotive effects on ion acceleration in the auroral zone, *Geophys. Res. Lett.*, *20*, 13, 1993.

Lysak, R. L., Feedback instability of the ionospheric resonant cavity, *J. Geophys. Res.*, *96*, 1553, 1991.

Mitchell, D. G., M. J. Engebretson, D. J. Williams, C. A. Cattel, and R. Lundin, Pc5 pulsations in the outer dawn magnetosphere seen by ISEE 1 and 2, *J. Geophys. Res.*, *95*, 967, 1990.

Mjølhus, E., On the modulational instability of hydromagnetic waves parallel to the magnetic field, *J. Plasma Phys.*, *16*, 321, 1976.

Pu, Z. Y., A. Kurth and G. Kremser, Plasma and magnetic field parameters at substorm onsets derived from GEOS 2 observations, *J. Geophys. Res.*, *97*, 19,341, 1992.

Rankin, R., B. G. Harrold, J. C. Samson, and P. Frycz, The nonlinear evolution of field line resonances in the Earth's magnetosphere, *J. Geophys. Res.*, *98*, 5839, 1993a.

Rankin, R., J. C. Samson, and P. Frycz, Simulations of driven field line resonances in the Earth's magnetosphere, *J. Geophys. Res.*, *98*, 21341, 1993b.

Ruohoniemi, J. M., R. A. Greenwald, K. B. Baker, and J. C. Samson, HF radar observations of Pc5 field line resonances in the midnight/early morning MLT sector, *J. Geophys. Res.*, *96*, 15,697, 1991.

Sakai, J., and B. U. O. Sonnerup, Modulational instability of finite amplitude dispersive Alfvén waves, *J. Geophys. Res.*, *88*, 9069, 1983.

Samson, J. C., D. D. Wallis, T. J. Hughes, F. Creutzberg, J. M. Ruohoniemi, and R. A. Greenwald, Substorm intensifications and field line resonances in the nightside magnetosphere, *J. Geophys. Res.*, *97*, 8495, 1992.

Seyler, C. E., A mathematical model of the structure and evolution of small scale discrete auroral arcs, *J. Geophys. Res.*, *95*, 17,199, 1990.

Trakhtengertz, V. Yu., and A. Ya. Feldstein, Quiet auroral arcs: Ionospheric effect of magnetospheric stratification, *Planet. Space Sci.*, *32*(2), 127, 1984.

Wong, H. K., and M. L. Goldstein, Parametric instabilities of circularly polarized Alfvén waves including dispersion, *J. Geophys. Res.*, *91*, 5617, 1986.

P. Frycz, R. Rankin and J.C. Samson, Department of Physics, Canadian Network for Space Research, University of Alberta, CW-005 Biological Sciences Building, Edmonton, Alberta, Canada T6G 2E9.
(e-mail: frycz@space.ualberta.ca; rankin@space.ualberta.ca; samson@space.ualberta.ca)

V.T. Tikhonchuk, P.N. Lebedev Physics Institute, Russian Academy of Science, Moscow, Russia.

(Received April 5, 1994; revised June 13, 1994; accepted June 20, 1994.)